

## ABSTRACT

Title of Document: COBALTFERRITE-BARIUMTITANATE  
SOL-GEL BIFERROICS

Lei Zheng, Master of Science, 2006

Directed By: Professor, Manfred Wuttig, Department of  
Materials Science and Engineering

Multiferroic materials that display a coexistence of ferroelectric and ferromagnetic responses attract interest because of their potential for several novel device applications. In multiferroic composite, electromagnetic coupling is facilitated by elastic interaction between ferroelectric and ferromagnetic components via piezoeffect and magnetostriction. The goal of our research is to prepare magnetoelectric composite using sol-gel technology. This method consisted of two steps, preparing a mixture of the synthesized ferromagnetic and ferroelectric nanoparticles at certain ratio and sintering. The nanoparticles were characterized by Differential Thermal Analysis and Thermogravimetric Analysis. The crystal structure and microstructure were studied by X-ray Diffraction and Scanning Electron Microscopy, respectively. Dielectric Analysis, Superconducting Quantum Interference Device and Vibrating Sample Magnetometer were used to examine the electric and magnetic properties. BTO-CFO multiferroics whose electric permittivity increased by magnetization were successfully synthesized by this method.

COBALTFERRITE-BARIUMTITANATE SOL-GEL BIFERROICS

By

Lei Zheng

Thesis submitted to the Faculty of the Graduate School of the  
University of Maryland, College Park, in partial fulfillment  
of the requirements for the degree of  
Master of Science  
2006

Advisory Committee:  
Professor Manfred Wuttig, Chair/Advisor  
Professor Isabel K. Lloyd  
Professor James Cullen



## Dedication

To the memory of my father

To my mother and my husband

## Acknowledgements

I would like to express my sincere thanks to my advisor, Professor Manfred Wuttig, who has given me the opportunity to work in his group, for his advice, encouragement, and support on research and also support during my hard time of my life.

I would like to thank Professor Isabel K. Lloyd who supplied a good environment for me to do my research in her lab. Also, I would especially like to thank to another committee member Professor James Cullen for his efforts on my behalf.

I appreciate these friends Dr. Liyang Dai, Dr. Zhengkun Ma, Dr. Jianhua Li, Dr. Li ling for their helpful discussion and assistance in my research and for their support in my life. Also, I would like to thank my colleagues Peng Zhao, Shenqiang Ren.

My deep gratitude goes to my parents. Without their continuous encouragement, support and understanding, it would have been impossible for me to accomplish all of my study and research.

Finally, I would like to thank my husband, Xin Zhang who gives me many suggestions in my experiment. His love and encouragement is my endless power to keep going ahead.

# Table of Contents

Dedication.....	ii
Acknowledgements.....	iii
Table of Contents.....	iv
List of Tables.....	vi
List of Figures.....	vii
List of Figures.....	vii
Chapter 1: Introduction.....	1
1.1 Biferroic Materials.....	1
1.2 Ferromagnetism.....	4
1.2.1 CoFe <sub>2</sub> O <sub>4</sub> .....	5
1.3 Ferroelectricity.....	6
1.3.1 BaTiO <sub>3</sub> Perovskite Structure.....	9
1.4 Composite Materials.....	9
1.4.1 Magnetoelectric Effect in Composite Materials.....	11
1.4.2 BaTiO <sub>3</sub> – CoFe <sub>2</sub> O <sub>4</sub> System.....	12
1.5 Sol-Gel Technology.....	13
1.6 Goal of Research.....	14
Chapter 2: Synthesis of BaTiO <sub>3</sub> -CoFe <sub>2</sub> O <sub>4</sub> .....	16
2.1 BaTiO <sub>3</sub> -CoFe <sub>2</sub> O <sub>4</sub> Synthesis.....	16
2.1.1 Preparation of BaTiO <sub>3</sub> /CoFe <sub>2</sub> O <sub>4</sub> (molar ratio: 4:1) Wet Gels.....	16
2.1.2 Preparation of BaTiO <sub>3</sub> /CoFe <sub>2</sub> O <sub>4</sub> (3:1, 1:1 and 1:3) Wet Gels.....	18
2.2 Drying and Sintering.....	19
Chapter 3: Characterization.....	21
3.1 Thermal Analysis: DTA, TGA.....	21
3.1.1 Differential Thermal Analysis.....	21
3.1.2 Thermogravimetry Analysis.....	22
3.2 Structure Analysis: XRD, SEM, EDS.....	22
3.2.1 X-ray Diffraction.....	22
3.2.2 Scanning Electron Microscopy.....	24
3.2.3 Energy Dispersive Spectroscopy.....	25
3.3 Magnetic Measurement: SQUID and VSM.....	25
3.3.1 Superconducting Quantum Interference Device.....	25
3.3.2 Vibrating Sample Magnetometer.....	25
3.4 Electric Measurement: Dielectric Analyzer (DEA).....	26
Chapter 4: Results and Discussion.....	27
4.1 TGA and DTA Data.....	27
4.2 XRD Results.....	29
4.3 SEM and EDS Measurements.....	32
4.4 Ferromagnetic Measurement.....	34
4.5 DEA Measurement.....	36
4.6 Discussion.....	37
Chapter 5: Conclusion.....	38

Chapter 6: Future Research.....	39
6.1 Embedded Particles with Two Phases .....	39
6.2 Films with Embedded Second Phase Particles .....	39
Appendix:.....	41
Bibliography: .....	43

## List of Tables

Table 1. 1 History of Biferroics.....	1
Table 2. 1 BaTiO <sub>3</sub> -CoFe <sub>2</sub> O <sub>4</sub> molar ratio.....	16



## List of Figures

Fig.1.1	Hysteresis loop showing magnetization switching in ferromagnetic materials.....	5
Fig.1.2	Schematic of the spinel structure, showing octahedral and tetrahedral sites occupied by A and B cations. ....	6
Fig.1.3	Ferroelectric hysteresis loop (schematic). ....	8
Fig.1.4	Perovskite structure.....	9
Fig.1.5	Sol-gel technologies and their products.....	14
Fig.2.1	Synthesis layout.....	17
Fig.2.2	Single-action pressing.....	19
Fig.2.3	Illustration for sintering. ....	20
Fig.3.1	Diagram of incident angle and reflecting angle with respect to the normal of the diffracting for X-ray diffraction. ....	23
Fig.4.1	DTA of BaTiO <sub>3</sub> -CoFe <sub>2</sub> O <sub>4</sub> precursors in air. ....	28
Fig.4.2	DTA and TGA results for 25%BaTiO <sub>3</sub> -75%CoFe <sub>2</sub> O <sub>4</sub> precursor. Heat treatment at 5°C/min in DTA and 20°C/min in TGA in air.....	28
Fig.4.3	XRD pattern of BTO sintered at 1100°C.....	30
Fig.4.4	XRD pattern of CFO sintered at 1100°C.....	30
Fig.4.5	XRD patterns of the samples with a composition of 80%BaTiO <sub>3</sub> -20% CoFe <sub>2</sub> O <sub>4</sub> , heat-treated at 500°C, 700°C, 900°C and 1100°C respectively. P is BaTiO <sub>3</sub> perovskite phase. S is CoFe <sub>2</sub> O <sub>3</sub> spinel phase.....	31
Fig.4.6	XRD patterns of the samples with a composition of (A) 80%BaTiO <sub>3</sub> -20%CoFe <sub>2</sub> O <sub>4</sub> , (B) 75%BaTiO <sub>3</sub> -25%CoFe <sub>2</sub> O <sub>4</sub> , (C) 50%BaTiO <sub>3</sub> -50%CoFe <sub>2</sub> O <sub>4</sub> , (D) 25%BaTiO <sub>3</sub> -75%CoFe <sub>2</sub> O <sub>4</sub> heat-treated at 1100°C respectively. P is BaTiO <sub>3</sub> perovskite phase. S is CoFe <sub>2</sub> O <sub>3</sub> spinel phase.....	32
Fig.4.7	Typical SEM micrograph of the polished surface of the 25%BaTiO <sub>3</sub> -75%CoFe <sub>2</sub> O <sub>4</sub> composite sample sintered at 1100°C for 2 hours. ....	33
Fig.4.8	The result of EDS of the 25%BaTiO <sub>3</sub> -75%CoFe <sub>2</sub> O <sub>4</sub> composite. ....	34
Fig.4.9	M vs. H for 25%BaTiO <sub>3</sub> -75%CoFe <sub>2</sub> O <sub>4</sub> composite and pure CoFe <sub>2</sub> O <sub>4</sub> at 300K.....	35
Fig.4.10	M vs. T response for 25%BaTiO <sub>3</sub> -75%CoFe <sub>2</sub> O <sub>4</sub> composite. ....	35
Fig.4.11	DEA for 25%BaTiO <sub>3</sub> -75%CoFe <sub>2</sub> O <sub>4</sub> composite with and without magnetized. ....	36
Fig.6.1	Illustration of embedded particles with two phases.....	40

# Chapter 1: Introduction

## 1.1 Biferroic Materials and Magnetoelectric Materials

Ferroic materials are those that display a spontaneous magnetization (ferromagnetic), polarization (ferroelectric) and strain (ferroelastic, shape memory alloy). Materials that possess two “ferro” properties simultaneously are called “biferroics”. There are three kinds of biferroic materials, Electroelastic material, Magnetoelastic material and Magnetoelectric material. Table1.1 presents a brief summary of the history of biferroic materials.

Table1.1 History of Biferroics

	Biferroic	Alloys	Year	Name	T <sub>c</sub> (°C)	Reference
Natural	Electroelastic	PMN	1970	Cross	100	1
	Magnetoelastic	Ni <sub>2</sub> MnGa	1995	O’Handley	100	2
		FePd	1995	Wuttig	40	3
		Boracide	1960	Schmid		4
		YbMnO <sub>5</sub>	2003	Cheong	-230	5
Artificial Composite	Magnetoelectric	Terfenol-PVDF	2002	Wuttig	>RT	6
		Terfenol-PZT	2002	Viehland	>RT	7
		BTO-CFO (PLD)	2003	Ramesh	RT	8
		BTO-CFO (Sol-Gel)	2006	Wuttig	RT	

Electroelastic materials are essentially piezoelectric materials, which have been widely studied and used in many applications. Magnetoelastic materials are magnetic shape memory alloys, which has also been widely studied. Regarding the magnetoelectric materials, little knowledge has been gathered. The magnetoelectric materials simultaneously possess ferromagnetic properties, which

will be discussed in section 1.2, and ferroelectric properties, which will be discussed in section 1.3. Because of the coupling between magnetization and polarization, a wide range of application can be proposed. Possible applications of magnetoelectric materials include magnetic-electric energy converting components, solid state nonvolatile memory, multi-state memory which can find application in quantum computing area and electric/optical polarization components which can find applications in communication, light computing and solid state memories based on spintronics.<sup>9, 10</sup>

The magnetoelectric effect was firstly predicted by P. Curie in 1894.<sup>11</sup> The first magnetoelectric material discovered was nickel iodine boracite,  $\text{Ni}_3\text{B}_7\text{O}_{13}\text{I}$ , in 1960's. However, due to the complexity of the boracite structure, little applications and understanding behind the phenomena was found. The other attempt to the magnetoelectric material was to replace certain cations in the ferroelectric perovskite oxide by magnetic cations. However, due to the dilution of the magnetic ions, these materials have Curie temperatures far below room temperature. Recently,  $\text{YbMn}_2\text{O}_5$  with a modified perovskite structure has been reported having magnetoelectric properties, but the Curie temperature is still far below room temperature. These two kinds of structures are the only possible structures for the magnetoelectric crystals. A lot of work has been done around these two structures and many modifications with different compositions have been reported, but no real application has been developed based on these crystals. There are two inherent problems with these crystals, one is low coupling efficient, and the other is low Curie temperature.

As described above, natural crystals of magnetoelectric materials were not suitable for common applications. Therefore, composites become the natural choice. If materials with magnetostriction and electrostriction were coupled together mechanically, the mechanical interaction between the magnetostriction phase and the electrostriction phase can lead to a functional magnetoelectric material. If a magnetic field is applied to such a composite, due to the magnetostriction effect, the ferromagnetic phase deforms. Because the electrostrictive phase is mechanically coupled with the magnetostriction phase, the electrostriction phase also deforms to adapt to the strain. As the electrostriction materials have piezoelectric effect, the spontaneous polarization of the electrostriction phase changes. If an electric field is applied to the composite, reverse effect will happen and the spontaneous magnetization changes. With this approach, several attempts have been made. One attempt was coupling of magnetostrictive metal, Terfenol, with electrostrictive polymer, Polyvinylidene Fluoride (PVDF). Terfenol was also used to couple with BaTiO<sub>3</sub>. These two attempts produced magneto-electric bulk materials.<sup>12, 13</sup> Another attempt was to couple CoFe<sub>2</sub>O<sub>3</sub> with BaTiO<sub>3</sub> by pulse laser deposition (PLD). This method can produce nanostructure films that can be integrated into an integrated circuit (IC). However, the drawback of PLD is this experiment method is expensive and slow. The major advantage of the composite approach over the single crystal approach in the engineering side is that the Curie temperatures of the material are expected to stay close to their bulk values. From the reported experimental data, the coupling coefficient is much higher than that of single phase crystals.

## ***1.2 Ferromagnetism***

Ferromagnetism is a phenomenon by which a material can exhibit a spontaneous magnetization. It is responsible for most of the magnetic behavior encountered in everyday life and is the basis for all permanent magnets. Electron spin and the Pauli Exclusion Principle are the physical origin of ferromagnetism.<sup>14</sup> The spin of an electron combined with its orbital angular momentum, results in a magnetic dipole moment and creates a magnetic momentum. Only atoms with partially filled shells with unpaired spins can exhibit a net magnetic moment in the absence of an external field, according to the response to the external magnetic field, the material can be classified into paramagnetism, ferromagnetism, antiferromagnetism and ferrimagnetism. Paramagnetic materials feature disordered orientations of the magnetic moments due to thermal fluctuations. Ferromagnetism is the strongest form of magnetic responses which is characterized by the parallel alignment of adjacent magnetic moments. In contrast, an antiferromagnetic behavior corresponds to an antiparallel alignment of equal moments. Finally, ferrimagnetism is characterized by antiparallel moments having different magnitudes and thus yielding a non-zero net magnetization.

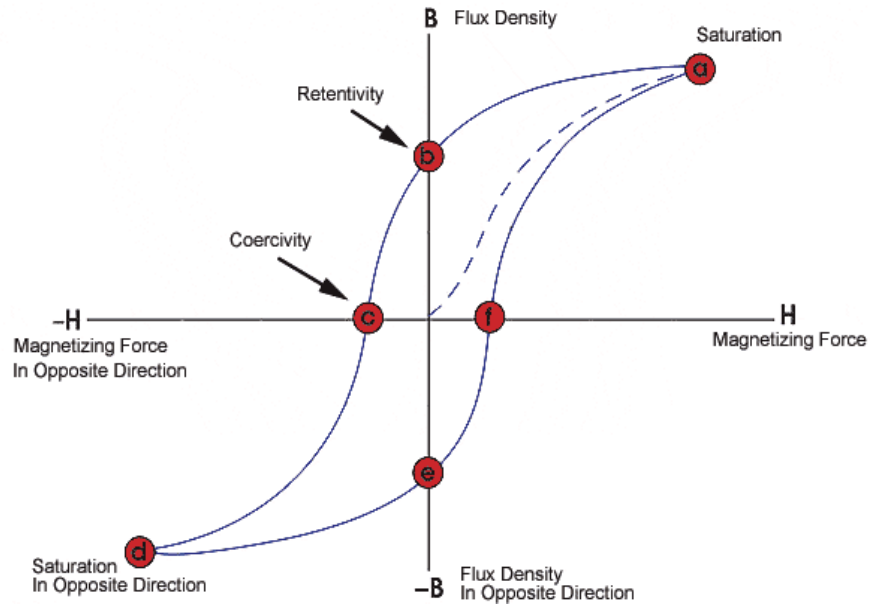


Fig.1.1 Hysteresis loop showing magnetization switching in ferromagnetic materials.

Ferromagnetics exhibit a hysteretic response to an external magnetic field, as shown in Fig.1.1. The saturation magnetization ( $M_s$ ), coercive field ( $H_c$ ) and remnant magnetization ( $M_r$ ) are all shown in the figure. Based on the value of a coercive field, magnetic materials are classified as either hard or soft magnets with large and small  $H_c$  accordingly.

### 1.2.1 Cobalt Ferrite ( $\text{CoFe}_2\text{O}_4$ )

$\text{CoFe}_2\text{O}_4$  is a ferromagnetic material, which belongs to the family of spinel structure (also called garnet structure). The spinel structure is named after the mineral spinel ( $\text{MgAl}_2\text{O}_4$ ) and has the general composition  $\text{AB}_2\text{O}_4$ . It is essentially cubic, with the O<sup>-</sup> ions forming an FCC lattice. The cations (usually metals) occupy 1/8 of the tetrahedral sites and 1/2 of the octahedral sites. There are 32 O<sup>-</sup> ions and 24 Cations in the unit cell, for a total of 56 atoms. The unit cell of spinel

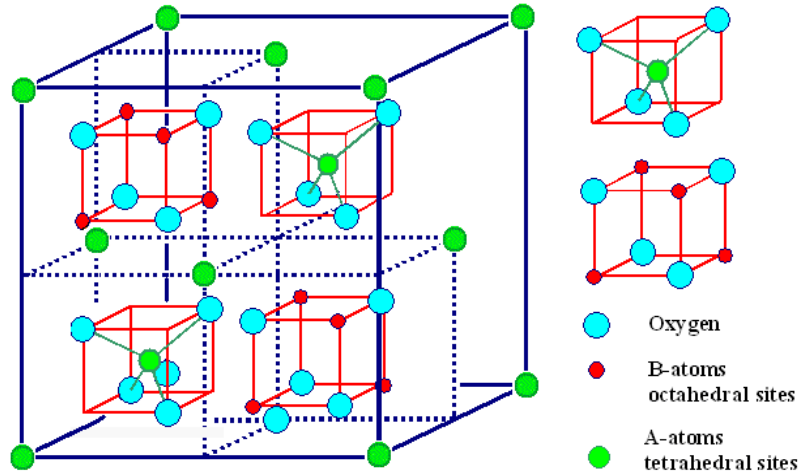


Fig.1.2 Schematic of the spinel structure, showing octahedral and tetrahedral sites occupied by A and B cations.

structure is illustrated in Fig.1.2. The Curie temperature of  $\text{CoFe}_2\text{O}_4$  is  $500^\circ\text{C}$ . Below  $T_C$ ,  $\text{CoFe}_2\text{O}_4$  exhibits the ferromagnetic properties.

$\text{CoFe}_2\text{O}_4$  also has high magnetostriction coefficient. The linear magnetostrictive strain of it is up to around  $-200 \times 10^{-6}$ , while other ferrites have a value at an order smaller than  $\text{CoFe}_2\text{O}_4$ .<sup>15</sup> Therefore, it is a potential candidate for the electromagnetic composites.

### ***1.3 Ferroelectricity***

Ferroelectric materials have a spontaneous electric polarization. They have been studied since over a century ago when large piezoelectric constants were observed in Rochelle salt.<sup>16</sup> For the past few decades, ferroelectric materials have received a great amount of interests because of their various uses in a range of applications, including transducers and actuators, capacitors and memory applications.

A ferroelectric material possesses at least two equilibrium orientations of the spontaneous polarization vector in the absence of an external electric field, and the spontaneous polarization can be switched by an electric field. The polar character of the orientation states should represent an absolutely stable configuration in null field.<sup>17</sup> The polarization as a function of the applied field for a ferroelectric crystal is a hysteresis loop as shown in Fig.1.3, which is a sign for the ferroelectric state. As the applied external field is switched off, a spontaneous polarization  $P_s$  persists. A reverse field  $-E_c$ , called coercive field, has to be applied to bring the polarization of the crystal back to zero. If the reverse field is increased further the polarization of the crystal is reversed. This is one of the important features of ferroelectrics with respect to applications. The ferroelectricity of a crystal disappears as it is heated up to Curie temperature  $T_c$ . Above  $T_c$  the crystal is said to be paraelectric.

It is well known that any crystal can be classified in as one of the thirty-two crystal classes (point groups) according to the symmetry elements, which it possesses. A study of these thirty-two classes reveals that eleven of them are characterized by the existence of a center of symmetry: they are called centrosymmetric. A centrosymmetric crystal can possess no polar properties. The remaining twenty-one crystal classes do not have a center of symmetry; they are non-centric. The absence of a center of symmetry makes it possible for crystals in these classes to have one or more polar axes and to show vectorial or tensorial properties. With one exception (i.e., the cubic class 432 which, without a center of symmetry, but has other symmetry elements that destroy polarity), all classes



devoid of a center of symmetry exhibit the piezoelectric effect that is defined by a change in electric polarity under applied stress, and vice versa, that is the converse piezoelectric effect.

Out of the twenty piezoelectric classes, ten are characterized by the fact that they have a unique polar axis. Crystals in these classes are called polar because they are spontaneously polarized. The value of the spontaneous polarization is dependent on temperature; thus, if the temperature of the crystal is altered a change in the polarization occurs and electric charges can be observed on those crystal faces that are perpendicular to the polar axis. This is the pyroelectric effect. The ten crystal classes with a unique polar axis are also called pyroelectric classes. Ferroelectric crystals belong to the pyroelectric family, but they are a subclass in which the direction of the spontaneous polarization can be reversed by external electric field.<sup>18</sup>

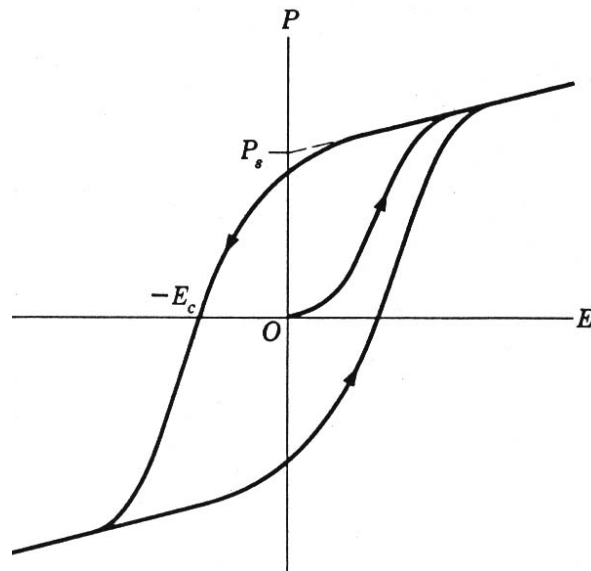


Fig.1.3 Ferroelectric hysteresis loop (schematic).

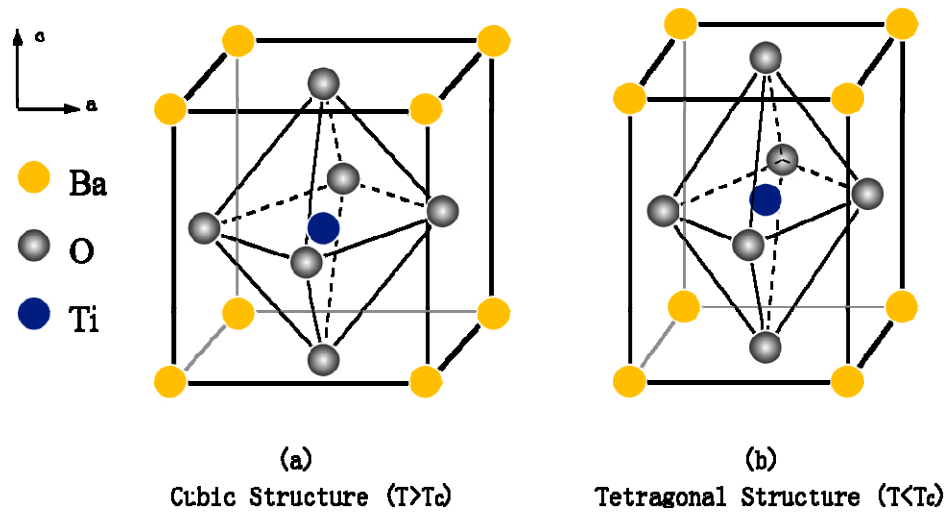


Fig.1.4 Perovskite structure.

### 1.3.1 Barium Titanate ( $\text{BaTiO}_3$ )

$\text{BaTiO}_3$  is a ferroelectric material with a perovskite structure as shown in Fig.1.4. It is the first discovered piezoelectric ceramic<sup>19</sup>.  $\text{BaTiO}_3$  is cubic structure above Curie temperature,  $120^\circ\text{C}$ . Cubic  $\text{BaTiO}_3$  is non-ferroelectric because the centers of positive and negative charges overlap as the ions are symmetrically arranged in the unit cell. Below  $T_c$ , it has tetragonal structure, in which the  $\text{O}^{2-}$  ions in the  $\text{BaTiO}_3$  crystal are shifted in the negative c-direction, while the  $\text{Ti}^{4+}$  ions are shifted in the positive c-direction. It results an electric dipole along the c-axis. Therefore  $\text{BaTiO}_3$  is ferroelectric in tetragonal structure.

### 1.4 Composite Materials

Composite materials are composed of two or more phases with different physical and chemical properties. Suchtelen divides the physical properties of

composite systems into two categories: sum properties and product properties.<sup>20</sup>

Sum property: that is a weighted sum of the contributions from the individual component phases, proportional to the volume or weight fractions of these phases in the composite. Physical quantities, such as density and resistivity are sum properties. The schematic representation is written as.

$$\left. \begin{array}{l} \text{Phase 1: } A \rightarrow B_1 \\ \text{Phase 2: } A \rightarrow B_2 \end{array} \right\} A \rightarrow B^* \quad (\text{Eq. 1.1})$$

Product property: that is reflected in the composite structure but are absent in the individual phases. In a biphasic composite material, if one phase exhibits a property  $A \rightarrow B$  (application of an independent variable  $A$  resulting in an effect  $B$ ) with a proportionality tensor  $dB/dA = X$  (maybe a constant or dependent on  $A$  or  $B$ ) and the second phase exhibits a property  $B \rightarrow C$  with a proportionality tensor  $dC/dB = Y$ , then the composite will exhibit a property  $A \rightarrow C$  which is absent in either of the initial phases. The property  $A \rightarrow C$  is called a product property of the composite. A typical example is the magnetoelectric effect in a composite material with one magnetostrictive and one piezoelectric phase such as  $\text{BaTiO}_3\text{-CoFe}_2\text{O}_4$  composite. A magnetic field induces a magnetostriction, which distorts the piezoelectric phase to generate an electric field.

$$\left. \begin{array}{l} \text{Phase 1: } A \rightarrow B \\ \text{Phase 2: } B \rightarrow C \end{array} \right\} A \rightarrow C \quad (\text{Eq. 1.2})$$

Depending on the application, the appropriate properties of the individual phases can be invoked to design a composite that will have a sum property or a product property.<sup>21</sup>

### 1.4.1 Magnetoelectric Effect on Multiferroic Composite Materials

The magnetoelectric effect is defined as a coupled two-field effect,<sup>22</sup> in which an application of a magnetic field induces an electric polarization. This is called “magnetically” induced magnetoelectric effect and denoted by  $ME_H$ . The effect in which an application of electric induces a magnetization is called “electrically” induced magnetoelectric effect and denoted by  $ME_E$ . Those effects have first been observed in  $Cr_2O_3$  single-phase material.<sup>23, 24, 25</sup> Later some other single-phase materials have been investigated for the ME effect.<sup>26, 27, 28, 29, 30, 31</sup>

The ME effect in composite systems has been suggested by Suchetelene of the Philips Laboratory as a product property between a Piezomagnetic and a piezoelectric materials. A suitable combination of two phases can yield the desirable property such as a combination of piezomagnetic and piezoelectric phases or a combination of magnetostrictive and piezoelectric phases. In 1978, Boomgaard<sup>32</sup> outlined the conceptual points inherent to the ME effect in composites. These can be summarized as (i) Two individual phases should be in equilibrium (ii) Mismatching between grains should not be present (iii) Magnitude of the magnetostriction coefficient of piezomagnetic or magnetostrictive phase and magnitude of the piezoelectric coefficient of the piezoelectric phase must be greater than both of the constituent phases respectively (iv) Accumulated charge must not leak through the piezomagnetic or magnetostrictive phase (v) Deterministic strategy for poling of the composites. At present various composites have been reported such as  $Ni (Co, Mn)Fe_2O_4$ - $BaTiO_3$ ,  $CoFe_2O_4$ - $BaTiO_3$ ,  $NiFe_2O_4$ - $BaTiO_3$ ,  $LiFe_5O_8$ - $BaTiO_3$ ,  $CoFe_2O_4$ - $Bi_4Ti_3O_{12}$  etc.<sup>33</sup>

### 1.4.2 BaTiO<sub>3</sub> – CoFe<sub>2</sub>O<sub>4</sub> System

BaTiO<sub>3</sub> is a typical ferroelectric material with large piezoelectricity; CoFe<sub>2</sub>O<sub>4</sub> is ferromagnetic with large magnetostriction. Composites of BaTiO<sub>3</sub>-CoFe<sub>2</sub>O<sub>4</sub> combine the ferroelectricity and ferromagnetism. The magnetoelectric coupling effect is through stress mediation. When a magnetic field is applied to the composite, there is stress generated by the CoFe<sub>2</sub>O<sub>4</sub> due to its magnetostriction. Such a stress can create an electric field in the BaTiO<sub>3</sub> due to its piezoelectricity. The reverse process is also possible.

The first attempt to fabricate a multiferroic composite through the eutectic crystallization of the mixture of BaTiO<sub>3</sub> and CoFe<sub>2</sub>O<sub>4</sub> was reported by J. Van Suchtelen in 1972. The 62%BaTiO<sub>3</sub>-38%CoFe<sub>2</sub>O<sub>4</sub> composites were synthesized by unidirectional solidification which is a method that has been used to produce an anisotropic composite directly from the melt. However, this process requires high temperature and a critical control over the composition especially when one of the components (oxygen) is gas, and unexpected third phase can appear in the composites.

Sintered magnetoelectric composites are an alternative to the *in-situ* eutectic composite formation. Sintered composite materials are much cheaper and easier to prepare. Moreover, their preparation offers several advantages: (1) the free choice of the molar ratio of constituent phase; (2) the independent choice of the grain size of each of the phases in the starting mixture; (3) the free choice of the sintering temperature; (4) the fact that the existence of a eutectic point, a eutectic gutter, or a eutectoid phase between the two desired phases is not a

prerequisite.

### ***1.5 Sol-Gel Technology***

The sol-gel process is a versatile solution process for making ceramic and glass materials. In general, the sol-gel process involves the transition of a system from a liquid “sol” into a solid “gel” phase. Applying the sol-gel process, it is possible to fabricate ceramic or glass materials in a wide variety of forms: ultra-fine or spherical shaped powders, thin film coatings, ceramic fibers and microporous inorganic membranes. An overview of the sol-gel process is presented in a simple graphic work as below in Fig.1.5.

The starting materials used in the preparation of the "sol" are usually inorganic metal salts or metal organic compounds such as metal alkoxides. In a typical sol-gel process, the precursor is subjected to a series of hydrolysis and polymeration reactions to form a "sol". Further processing of the "sol" enables one to make ceramic materials in different forms. Thin films can be produced on a piece of substrate by spin-coating or dip-coating. When the "sol" is cast into a mold, a wet "gel" will form. With further drying and heat-treatment, the "gel" is converted into dense ceramic or glass articles. If the liquid in a wet "gel" is removed under a supercritical condition, a highly porous and extremely low density material called "aerogel" is obtained. As the viscosity of a "sol" is adjusted into a proper viscosity range, ceramic fibers can be drawn from the "sol". Ultra-fine and uniform ceramic powders are formed by precipitation, spray pyrolysis, or emulsion techniques.

Our research lies in using sol-gel technology to make the magnetoelectric

dense ceramics. There are many advantages including<sup>34, 35</sup>

- 1) Better homogeneity compared to traditional mixed powder technology;
- 2) High purity compared to mineral raw material sources;
- 3) Lower temperature processing and consolidation is possible.
- 4) More uniform phase distribution in multicomponent systems;
- 5) Better size and morphological control in powder synthesis.

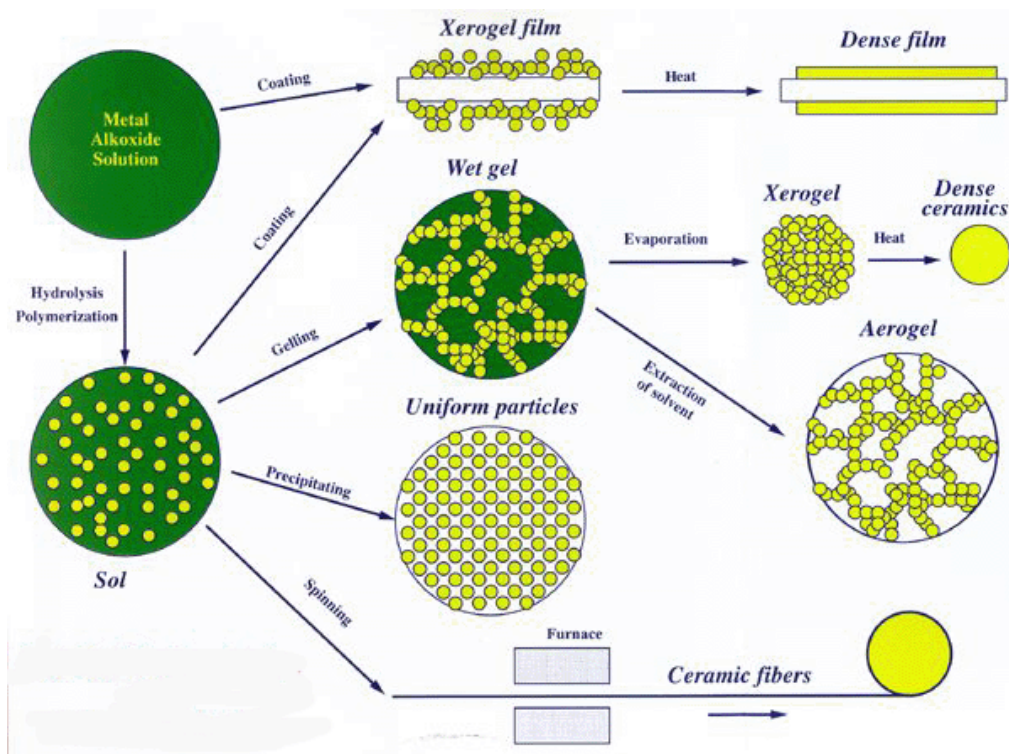


Fig.1.5 Sol-gel technologies and their products.<sup>36</sup>

### 1.6 Goal of Research

The goal of research presented in this monograph is to develop a new method to produce magnetoelectric composite materials. Barium Titanate and Cobalt Ferrite were selected as the ferroelectric and ferromagnetic phase,

respectively. These two materials were selected because their properties and structures have been widely studied and suitable for our research. In this research, sol-gel was selected as the synthesis method due to its low expense and ability to produce samples at different dimension and scale at large batch. The Curie temperature of Barium Titanate and Cobalt Ferrite phases was expected to stay close to their reported bulk values.

The coupling between ferromagnetic phase and ferroelectric was expected to be measurable by common experiment equipments at room temperature.



## Chapter 2: Synthesis of BaTiO<sub>3</sub>-CoFe<sub>2</sub>O<sub>4</sub>

In this thesis, the biferroic system of BaTiO<sub>3</sub>-CoFe<sub>2</sub>O<sub>4</sub> was studied. The composites were prepared by Sol-Gel technology.

### 2.1 BaTiO<sub>3</sub>-CoFe<sub>2</sub>O<sub>4</sub> Synthesis

Barium nitrate (>99%), Iron (III) nitrate nonahydrate (98.0-101.0%), Cobalt (II) nitrate hexahydrate (98.0-102.0%), Commercial available Ethylenediaminetetraacetic acid [EDTA, ((HO<sub>2</sub>CCH<sub>2</sub>)<sub>2</sub>NCH<sub>2</sub>CH<sub>2</sub>N(CH<sub>2</sub>CO<sub>2</sub>H)<sub>2</sub>)] (99%), and Citric acid anhydrous (>99.5%) were purchased from Alfa Aesar. Two kinds of butyl titanate that are Tetra-n-Butyl titanate (TnBT) and n-Butyltitanate polymer (BTP) were provided by DuPont with the trade name of Tyzor TnBT and Tyzor BTP respectively.

BaTiO<sub>3</sub>-CoFe<sub>2</sub>O<sub>4</sub> powders were prepared by the one-pot process.<sup>37</sup> Six kinds of molar ratio were studied in this thesis as shown in Table 2.1.

Table 2.1 BaTiO<sub>3</sub>-CoFe<sub>2</sub>O<sub>4</sub> molar ratio

BaTiO <sub>3</sub> % (x)	100%	80%	75%	50%	25%	0%
CoFe <sub>2</sub> O <sub>4</sub> % (y)	0%	20%	25%	50%	75%	100%
BaTiO <sub>3</sub> -CoFe <sub>2</sub> O <sub>4</sub> molar ratio (x : y)	1:0	4:1	3:1	1:1	1:3	0:1

#### 2.1.1 Preparation of BaTiO<sub>3</sub>/CoFe<sub>2</sub>O<sub>4</sub> (molar ratio: 4:1) Wet Gels

0.1 mol Ba(NO<sub>3</sub>)<sub>2</sub> was first dissolved into 500ml deionized water to get a transparent solution. 500 ml of 0.2M EDTA solution was adjusted to PH 6 by the addition of ammonia solution. After achieving complete dissolution, 0.1 mol

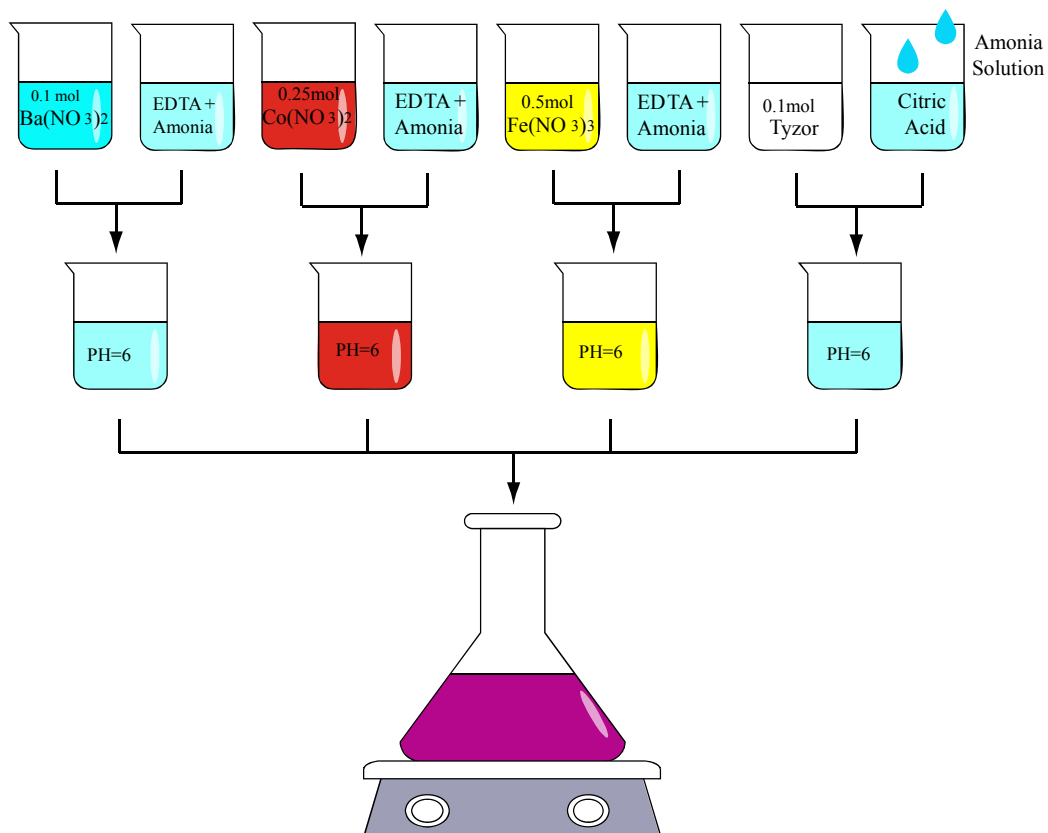


Fig.2.1 Synthesis layout.

$\text{Ba}(\text{NO}_3)_2$  was gradually added to EDTA. Then, the mixture was stirred until transparent. Fig.2.1 shows the synthesis layout.

Also, 0.25 mol red  $\text{Co}(\text{NO}_3)_2 \cdot 6\text{H}_2\text{O}$  and 0.5 mol violet  $\text{Fe}(\text{NO}_3)_3 \cdot 9\text{H}_2\text{O}$  were separately dissolved into 250ml deionized water to get the red transparent solution and yellow transparent solution. Co and Fe ion-containing solutions stabilized by EDTA were prepared in a similar manner as was used for Ba. EDTA forms a chelating structure with different metal ions and preventing the formation of an insoluble base or salt.

1000ml 2M citric acid  $[\text{HOCOCH}_2\text{C}(\text{OH})(\text{COOH})\text{CH}_2\text{COOH}]$  solution was adjusted to PH 6 by adding ammonia solution. 0.1 mol  $\text{Ti}[\text{O}(\text{CH}_2)_3\text{CH}_3]_4$

liquid was mixed with the citric acid solution. The molar ratio of  $\text{Ti}[\text{O}(\text{CH}_2)_3\text{CH}_3]_4$  to citric acid was 1:2. Complete dissolution was achieved by stirring.

The solutions containing Ba, Co, Fe and Ti components were then mixed together and sol-gel reaction gradually occurs while stirring the solution at  $70^\circ\text{C}$ .

### **2.1.2 Preparation of $\text{BaTiO}_3/\text{CoFe}_2\text{O}_4$ (3:1, 1:1 and 1:3) Wet Gels**

Using the method that we described above to prepare the  $\text{BaTiO}_3/\text{CoFe}_2\text{O}_4$  molar ratio: 4:1, three other molar ratios of  $\text{BaTiO}_3/\text{CoFe}_2\text{O}_4$  wet gels were prepared. The molar ratios of these were 3:1, 1:1 and 1:3. First, Ba, Co, Fe salts should be dissolved in water separately. Second, the stoichiometric amount of 0.2M EDTA solutions was prepared with the molar ratio of Ba component to EDTA being 1:1. The EDTA solution was adjusted PH 6 by adding an ammonia solution and then  $\text{Ba}(\text{NO}_3)_2$  was added to it. Similarly Co and Fe ion containing solutions stabilized by EDTA were prepared. The stoichiometric amount of butyl titanate was added to a 0.2M citric acid solution with PH 6 by adding an ammonia solution. The molar ratio of  $\text{Ti}(\text{OC}_4\text{H}_9)_4$  to citric acid is 1:2. Finally, the solution containing Ba, Co, Fe, Ti components were then mixed by mechanical stirring at  $70^\circ\text{C}$  until a viscous liquid appeared.

In order to compare the structure and the properties of different BTO-CFO samples in this study, the  $\text{BaTiO}_3$  and  $\text{CoFe}_2\text{O}_4$  samples were prepared by the same technique for calibration purpose.

## 2.2 Drying and Sintering

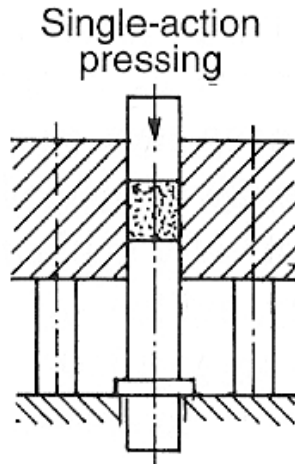


Fig.2.2 Single-action pressing.

The color of the viscous liquid was deep pink. It still contained impurities such as water and some organic materials and the state of particles in this liquid is still amorphous. In order to remove the water, solution was heated on the hot plate with a surface temperature above  $100^{\circ}\text{C}$  or placed in an oven at  $120^{\circ}\text{C}$  to remove water. After a few hours, a black hard dry mixture was retrieved. Then, the dried mixture was heat-treated above  $400^{\circ}\text{C}$  for 1 hour to investigate its phase development and achieved a fine porous powder.

The powders were milled for about two hours to produce coarse and irregular particles. Then, the disk-shaped samples were compressed at  $100^{\circ}\text{C}$ . A set of self-made single-action pressing stainless steel dies were used to make the disks as shown in Fig.2.1. The stainless steel dies were machined in the Engineering Machine Shop on campus. Two different shapes of samples were prepared. One is *1inch* in diameter for measuring the dielectric constant with a

dielectric analyzer (DEA). The other is 1cm in diameter with 1 or 2mm thickness for the other characterization.

The shaped samples were sintered at different temperatures in a tube furnace (Carbolite Company 1200°C CTF 12/65/550). The disk-shaped samples were first placed into a ceramic boat, and inserted into the tube. The boat should be of low thermal mass and should have feet to reduce the contact with the tube. Four different sintering temperatures were set as 500°C, 700°C, 900°C and 1100°C to compare the phases and identify the crystal structure. The samples were heated up at 2°C per minute to the set-point temperature; held at the set-point temperature for 2 hours; then allowed to air cool to room temperature as presented in Fig.2.3.

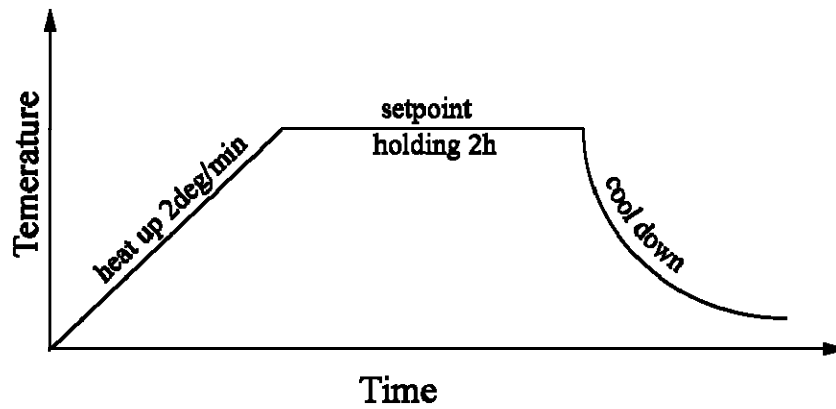


Fig.2.3 Illustration for sintering.

## Chapter 3: Characterization

In order to study the structure and properties of BaTiO<sub>3</sub>-CoFe<sub>2</sub>O<sub>4</sub> composite, thermal analysis, structure analysis, electric measurement and magnetic measurement were performed by DTA, TGA, XRD, SEM, EDS, DEA, SQUID and VSM.

### ***3.1 Thermal Analysis: DTA, TGA***

Thermal analysis was studied by Differential thermal analysis (DTA) and Thermogravimetry analysis (TGA).

#### **3.1.1 Differential Thermal Analysis**

DTA is a “fingerprinting” technique that provides information on the chemical reaction, phase transformations, and structural changes that occur in a sample during a heat-up or a cool-down cycle.

In this experiment, DTA-50 was used to monitor the decomposition process of the precursor. The test samples were placed into a specially shaped cup so the test material surrounded a thermocouple bead. The cup was made from a sintered, high purity alumina, which was relatively inert to the test sample. An identical cup as a reference cup was placed immediately beside the sample cup and went through the same heat treatment. Both cups were uniformly heated at a constant heating rate of 5°C/min from room temperature till 800°C/min. The DTA signal was the difference in temperature between these two thermocouple beads while the sample cups were heated. This temperature difference was due to heat capacity differences in the materials, and was constantly saved on the computer

along with the temperature inside the reference cup and the elapsed time. When a first order, second order transition, kinetic transition, or chemical reaction happens, there are changes in the heat capacities of the materials. These changes can be the “finger prints” of the transitions or reactions.

### **3.1.2 Thermogravimetry Analysis**

TGA uses heat to force reactions and physical changes in materials. TGA provides quantitative measurement of mass change in materials associated with transition, thermal degradation and chemical reaction. The TGA records change in mass from dehydration, decomposition, and oxidation of a sample with time and temperature. Characteristic thermogravimetric curves are given for specific materials and chemical compounds due to unique sequence from physicochemical reactions occurring over specific temperature ranges and heating rates. These unique characteristics are related to the molecular structure of the sample. By comparing the characteristic thermogravimetric curves and experimentally measured curve, the constituents of unknown samples can be identified indirectly.

### **3.2 Structure Analysis: XRD, SEM, EDS**

X-ray diffraction, Scanning Electron Microscopy (SEM) and Energy dispersive spectroscopy (EDS) were used to study the crystal structure, microstructure and composition, respectively.

#### **3.2.1 X-ray Diffraction**

The diffraction of X-rays by matter results from the combination of two different phenomena: (a) scattering by each individual atom, and (b) interference

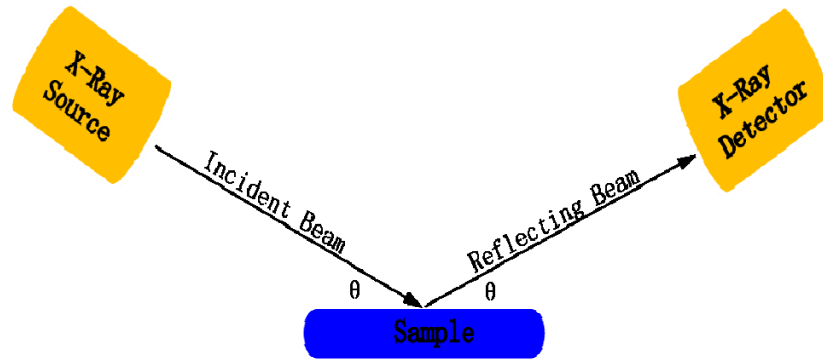


Fig.3.1 Diagram of incident angle and reflecting angle with respect to the normal of the diffracting for X-ray diffraction.

between the waves scattered by these atoms. This interference occurs because the waves scattered by the individual atoms are coherent with the incident wave, and therefore between themselves as shown in Fig.3.1.

In 1912, W. L. Bragg recognized a predictable relationship among several factors.

1. The distance between similar atomic planes in a mineral (the interatomic spacing) which we call the  $d$ -spacing and measure in angstroms.
2. The angle of diffraction which we call the theta angle and measure in degree. For practical reasons the diffractometer measures an angle twice that of the theta angle.
3. The wavelength of the incident X-radiation of Cu-K $_{\alpha}$ , symbolized by the Greek letter lambda and, in this thesis, equal to 1.54 angstroms.

These factors are combined in Bragg's Law:

$$n\lambda = 2d \sin \theta \quad (\text{Eq. 3.1})$$

Where  $n$  is an integer,  $\lambda$  is the wavelength of X-rays,  $d$  is the lattice interatomic



spacing and  $\theta$  is the diffraction angle.

The XRD was used in this thesis to identify the changes of the crystal structure in my samples after sintered at different temperature. The scanning of the  $2\theta$  angle was started at  $15^\circ$ , and ended at  $75^\circ$ . The scanning rate was  $0.5^\circ/\text{min}$ .

### **3.2.2 Scanning Electron Microscopy**

SEM is one of the most versatile instruments available for the examination and analysis of the microstructure characteristics of a solid. The most important reason for using the SEM is the high resolution that can be obtained when bulk sample are examined. Resolution on the order of 2 to 5 nm is now usually quoted for commercial instruments. Instruments with resolutions better than 1 nm are also available.

Another important feature of SEM is the three-dimensional appearance of the image. This is a direct result of the large depth of field, as well as the shadow-relief effects of the secondary and backscattered electron contrast. The greater depth of field of the SEM provides more information about the specimen. Most SEM micrograph has been produced with the magnification below  $8000\times 8000$  (diameters). At this magnification the SEM is operating well within its resolution capacities.

ESEM (ElectroScan) which was used in this thesis is a special type of SEM. It works under controlled environmental conditions and requires no conductive coating on the specimen. This makes it possible to examine specimens in their natural state.

### **3.2.3 Energy Dispersive Spectroscopy**

EDS is a standard procedure for identifying and quantifying elemental composition of sample areas as small as a few cubic micrometers. Characteristic X-rays are produced when a material is bombarded with electrons in an electron beam instrument, such as a scanning electron microscope (SEM). Detection of these X-ray can be accomplished by an energy dispersive spectrometer, which is a solid state device that discriminates among X-ray energies.

EDS provides the analytical information including qualitative analysis, quantitative analysis, line profile analysis and elemental mapping. The model of the EDS which was used in this thesis is JEOL JXA 840.

### ***3.3 Magnetic Measurement: SQUID and VSM***

Magnetic properties were identified by Superconducting quantum interference device (SQUID) and Vibrating Sample Magnetometer (VSM).

#### **3.3.1 Superconducting Quantum Interference Device**

SQUID is a device that measures minute changes in magnetic flux by means of a pair of Josephson junctions, often used to detect extremely small changes in magnetic fields, electric currents, and voltages.

#### **3.3.2 Vibrating Sample Magnetometer**

VSM is a basic research tool for determining the magnetic properties of a material. VSM was proposed first by Oosterhout<sup>38</sup> to study the structure of various magnetic materials. Today, it enjoys widespread use in the fields of superconductivity, thin films and crystal development. The VSM allows the

measurement of magnetic hysteresis loops, the studies of which form an important aspect of characterizing the magnetic materials themselves.

When a sample material is placed in a uniform magnetic field and made to undergo sinusoidal motion, a dipole moment will be induced in the material. The magnetic flux changes inducing an electrical signal in stationary coils positioned near the sample. This voltage induced is proportional to the magnetization of the sample.

### ***3.4 Electric Measurement: Dielectric Analyzer (DEA)***

DEA measures dielectric properties as a function of temperature, frequency and time. Dielectric properties define the capacity and conductivity of material. Capacitive properties determine the ability of the material to store electric charge. Conductive properties are proportional to the ability of charges to move in the material. Dielectric analyzer (DEA 2970) was used to measure dielectric properties of the bulk in this thesis.

## Chapter 4: Results and Discussion

BaTiO<sub>3</sub>-CoFe<sub>2</sub>O<sub>4</sub> composites with four different molar ratios were performed by XRD and DTA. 25%BaTiO<sub>3</sub>-75%CoFe<sub>2</sub>O<sub>4</sub> was characterized by TGA, SEM, EDS, DEA, SQUID and VSM.

### *4.1 TGA and DTA Data*

Fig.4.1 shows a series of precursors of DTA data from 80%BaTiO<sub>3</sub>-20%CoFe<sub>2</sub>O<sub>4</sub>, 75%BaTiO<sub>3</sub>-25%CoFe<sub>2</sub>O<sub>4</sub>, 50%BaTiO<sub>3</sub>-50CoFe<sub>2</sub>O<sub>4</sub> and 25%BaTiO<sub>3</sub>-75%CoFe<sub>2</sub>O<sub>4</sub>. Each precursor shows one small exothermic peak around 210°C which is followed by the two exothermic reactions. The precursors have decomposed almost completely after the third exothermic event, which indicates that the organic component of the gel has decomposed. Therefore, the precursors were heat-treated at 500°C for 2 hours before milling, compacting and sintering. Further weight loss at temperatures over 500°C may be due to the evaporation of Cobalt oxide.

The DTA/TGA curves for the 25%BaTiO<sub>3</sub>-75%CoFe<sub>2</sub>O<sub>4</sub> precursor are shown in Fig.4.2. The first weight loss before 100°C can be explained by the gradual evaporation of the water. The DTA events are accompanied by a second weight loss at 205°C and gradual decomposition from 230°C to 380°C. The gradual weight loss may be explained by gradual decomposition of the organic components.

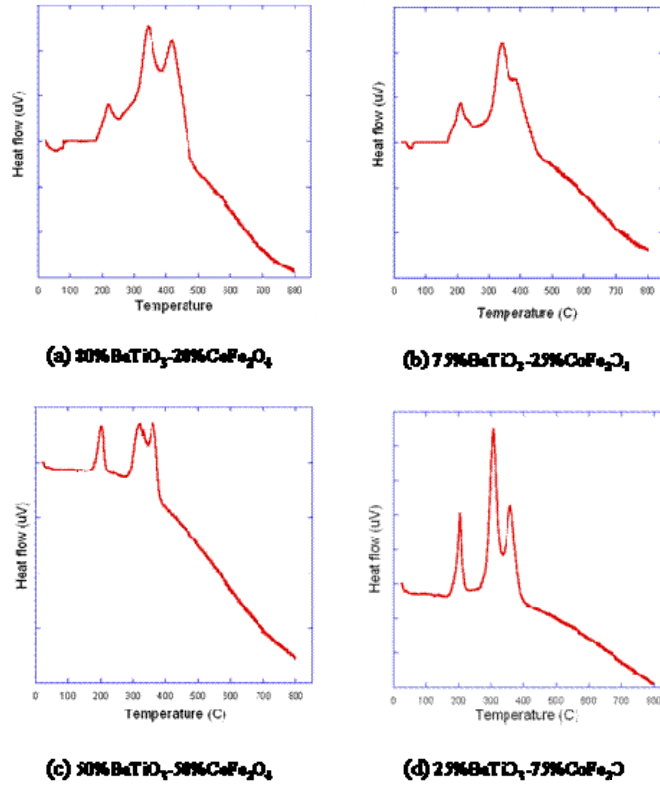


Fig.4.1 DTA of BaTiO<sub>3</sub>-CoFe<sub>2</sub>O<sub>4</sub> precursors in air.

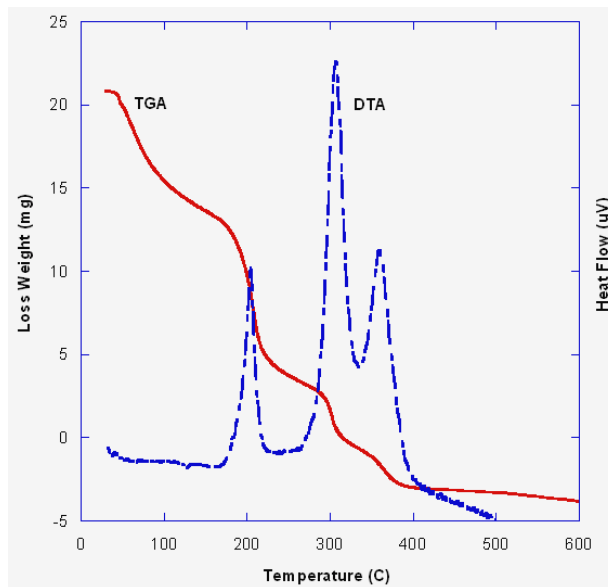


Fig.4.2 DTA and TGA results for 25%BaTiO<sub>3</sub>-75%CoFe<sub>2</sub>O<sub>4</sub> precursor. Heat treatment at 5°C/min in DTA and 20°C/min in TGA in air.

## **4.2 XRD Results**

In order to know what phases are present in the samples, it is very important to calibrate the reference data of each phase of BTO and CFO. The wavelength  $\lambda$  that was used in the XRD measurement was 1.54Å. With the knowledge that  $\lambda=1.54\text{\AA}$  and  $n=1$ ,  $2\theta$  can be calculated by Bragg's Law according to the atomic plane spacing  $d$  with respect to the phase hkl. Fig.4.3 and Fig.4.4 show the XRD patterns of BTO and CFO that were sintered at 1100°C, respectively. The peaks intensity provides information on the crystallinity and concentration of a material. Peak height is affected by orientation of crystals, quantity of crystals present and size of crystals. XRD can be used to determine the phase distribution of a material.<sup>39</sup> Different phases of a material will be identified by their crystallographic arrangement. There will be different XRD peaks for each phase of a material.<sup>40</sup>

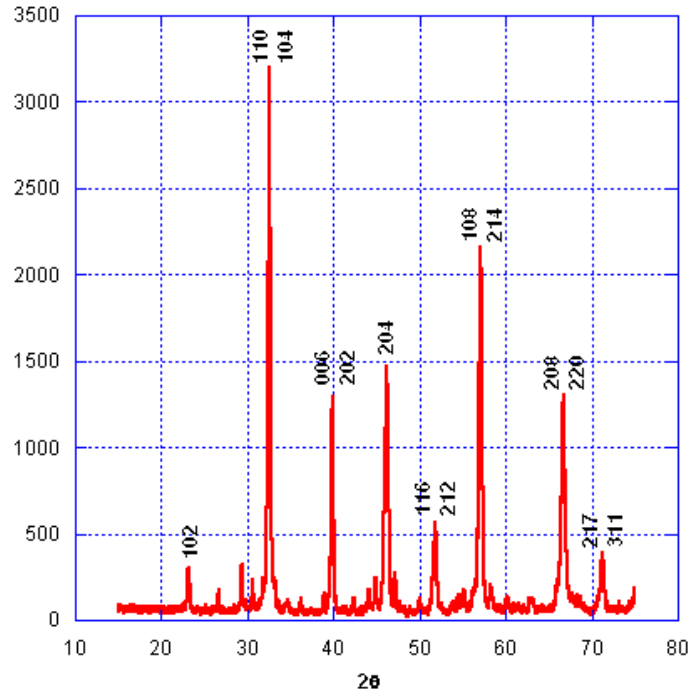


Fig.4.3 XRD pattern of BTO sintered at 1100°C.

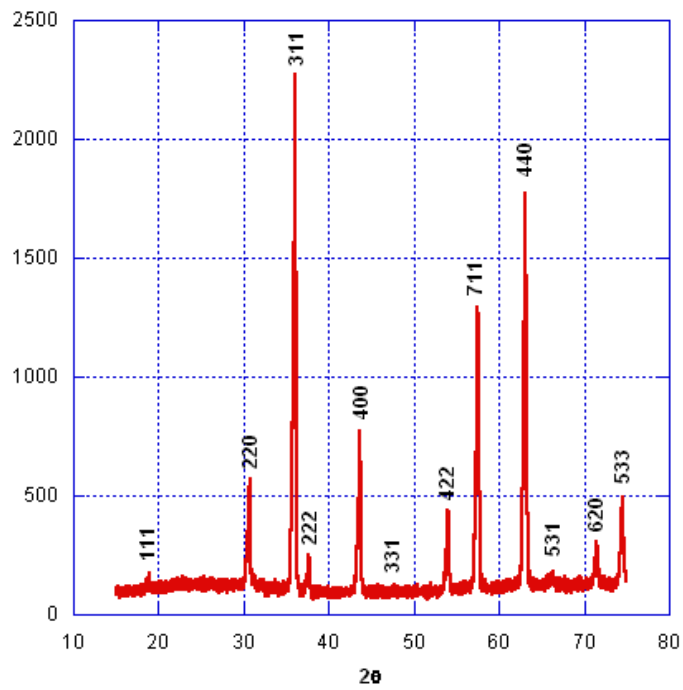


Fig.4.4 XRD pattern of CFO sintered at 1100°C.

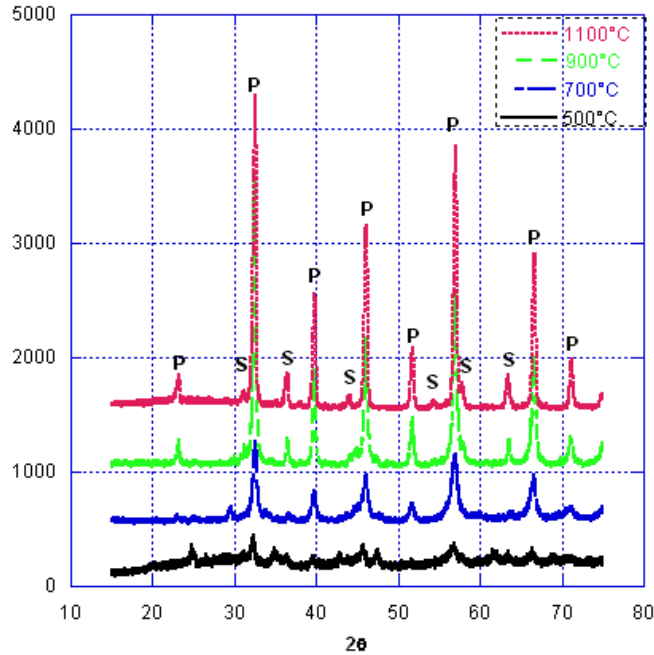


Fig.4.5 XRD patterns of the samples with a composition of 80%BaTiO<sub>3</sub>-20% CoFe<sub>2</sub>O<sub>4</sub>, heat-treated at 500°C, 700°C, 900°C and 1100°C respectively. P is BaTiO<sub>3</sub> perovskite phase. S is CoFe<sub>2</sub>O<sub>3</sub> spinel phase.

Fig.4.5 shows the XRD patterns of the samples with a composition of 80%BaTiO<sub>3</sub>-20% CoFe<sub>2</sub>O<sub>4</sub>, which was heat-treated 500°C, 700°C, 900°C and 1100°C respectively. The diffraction scans are from 15° to 75°. The X-ray diffractions showed that the precursor was of poor crystalline quality 500°C (black solid lines in Fig.4.5). When the sintering temperature reached 700°C, the crystalline BTO phase was formed, but the CFO phase was not well crystallized until 900°C. When the sample was sintered at 1100°C, only BTO and CFO phases were present without the inclusion of other phases. This is the prerequisite for presence of the magnetoelectric coupling effect. The peak intensities of the patterns indicated that the BTO phase was present in larger quantities than CFO phase.



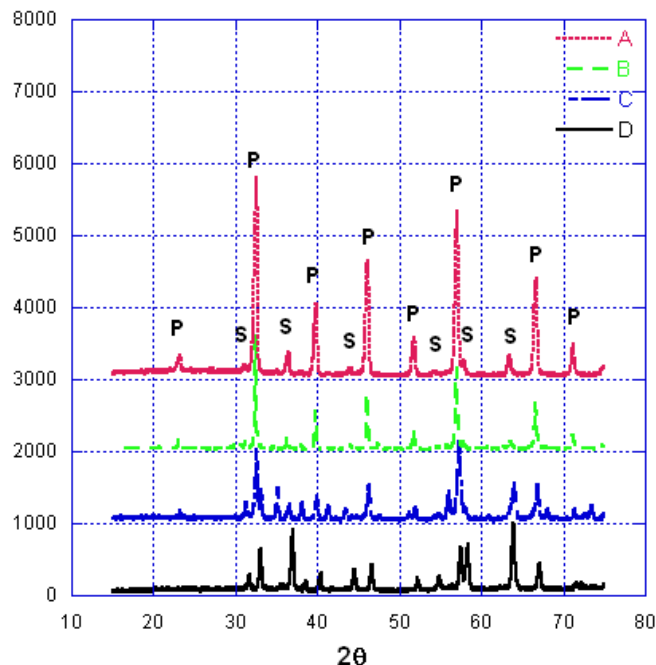


Fig.4.6 XRD patterns of the samples with a composition of (A) 80%BaTiO<sub>3</sub>-20%CoFe<sub>2</sub>O<sub>4</sub>, (B) 75%BaTiO<sub>3</sub>-25%CoFe<sub>2</sub>O<sub>4</sub>, (C) 50%BaTiO<sub>3</sub>-50%CoFe<sub>2</sub>O<sub>4</sub>, (D) 25%BaTiO<sub>3</sub>-75%CoFe<sub>2</sub>O<sub>4</sub> heat-treated at 1100°C respectively. P is BaTiO<sub>3</sub> perovskite phase. S is CoFe<sub>2</sub>O<sub>3</sub> spinel phase.

Fig.4.6 shows the XRD patterns of the BTO-CFO samples with four different compositions that were all heat-treated at 1100°C. The relative intensities of the patterns of the two phases are indicative of the composition of the BTO and CFO. Sample A and B indicated that the BTO is rich, while CFO is rich in sample C and D.

#### 4.3 SEM and EDS Measurements

The sintered samples were first polished and coated with Pt, then were examined by Scanning Electron Microscopy (SEM). SEM images of 25%BaTiO<sub>3</sub>-75%CoFe<sub>2</sub>O<sub>4</sub> sintered sample in Fig.4.7 showed that the average of the particles size is about 150nm.

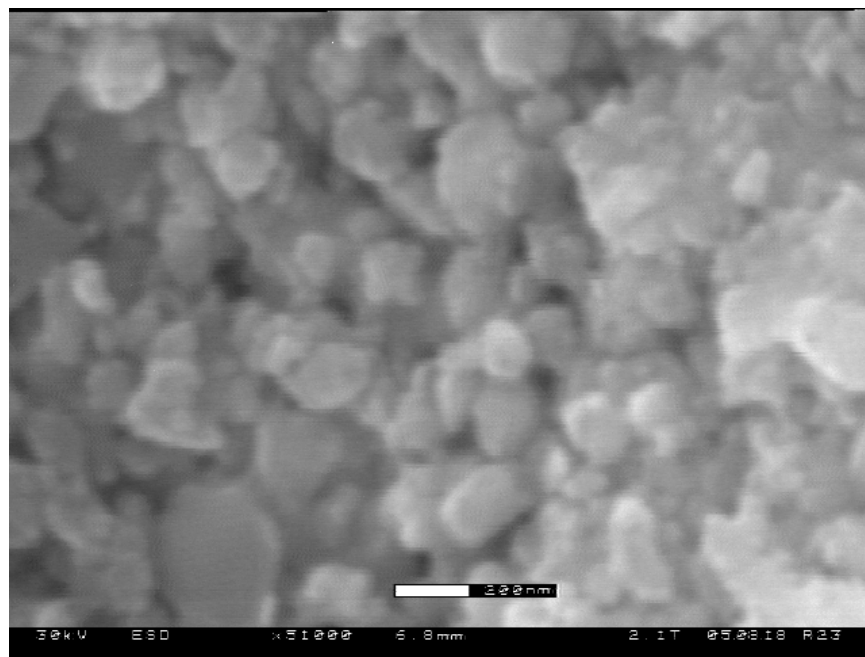
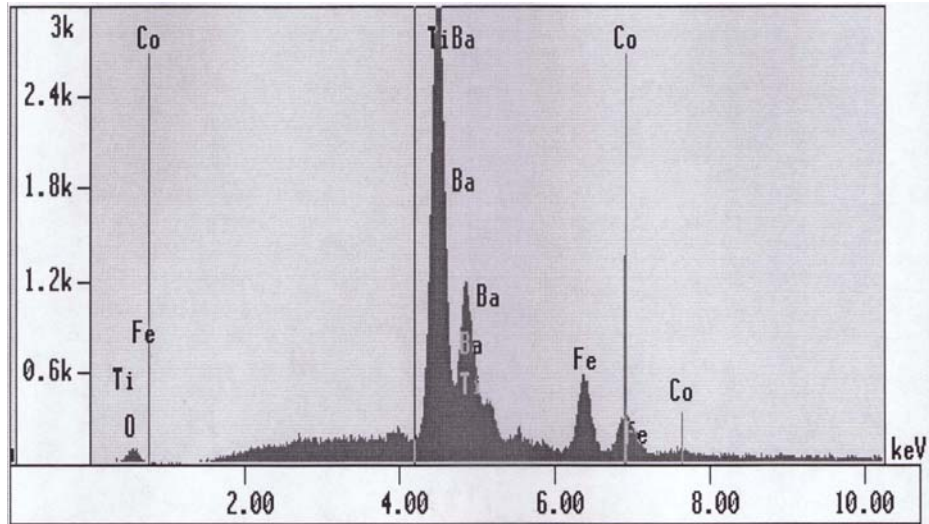
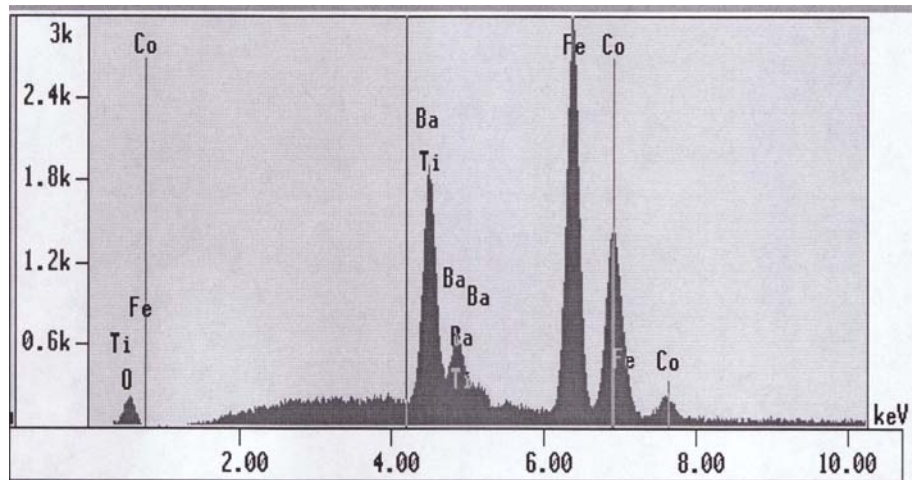


Fig.4.7 Typical SEM micrograph of the polished surface of the 25%BaTiO<sub>3</sub>-75%CoFe<sub>2</sub>O<sub>4</sub> composite sample sintered at 1100°C for 2 hours.

The results of the EDS are shown in Fig.4.8. The results of the matrix show strong Ba and Ti peaks with little appearance of Co and Fe peaks, which suggest that the composition of the matrix is BaTiO<sub>3</sub>; on the other hand, the phase in black was identified as CoFe<sub>2</sub>O<sub>4</sub>, since the EDS results exhibit strong Co and Fe peaks. In the results, probably Ba and Ti peaks appeared in white areas or Co and Fe peaks in black area and the reason why Co and Fe still can be observed in Ba and Ti area is that the incident electron beam could penetrate several micrometers in depth in the sample. Furthermore, XRD results (Fig.4.3-Fig.4.6) have confirmed that BaTiO<sub>3</sub> and CoFe<sub>2</sub>O<sub>4</sub> exist separately as pure and single phases.



(a)



(b)

Fig.4.8 The result of EDS of the 25%BaTiO<sub>3</sub>-75%CoFe<sub>2</sub>O<sub>4</sub> composite.

#### 4.4 Ferromagnetic Measurement

Ferromagnetic measurements were carried out on Superconducting Quantum Interference Device (SQUID) magnetometer and vibrating sample magnetometer (VSM). The magnetic hysteresis loop of 25%BaTiO<sub>3</sub>-75%CoFe<sub>2</sub>O<sub>4</sub> composite and the pure CoFe<sub>2</sub>O<sub>4</sub> is shown in Fig.4.9.

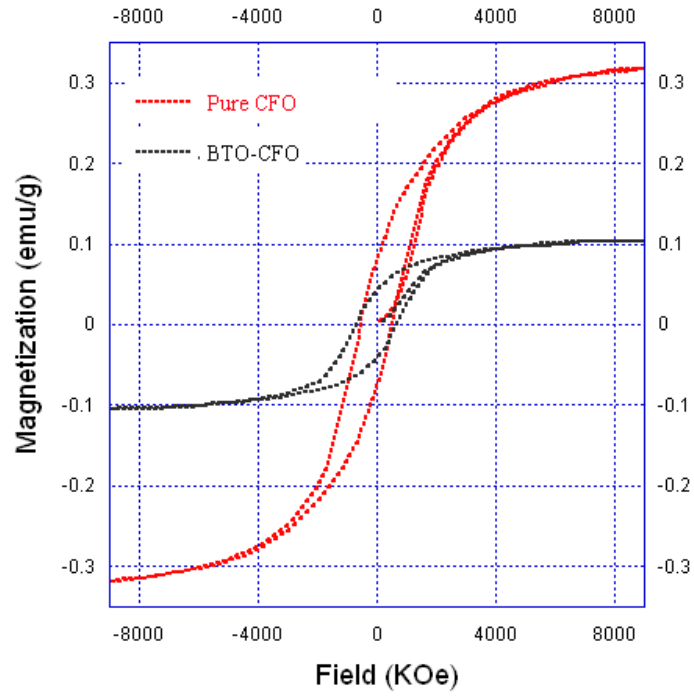


Fig.4.9 M vs. H for 25%BaTiO<sub>3</sub>-75%CoFe<sub>2</sub>O<sub>4</sub> composite and pure CoFe<sub>2</sub>O<sub>4</sub> at 300K.

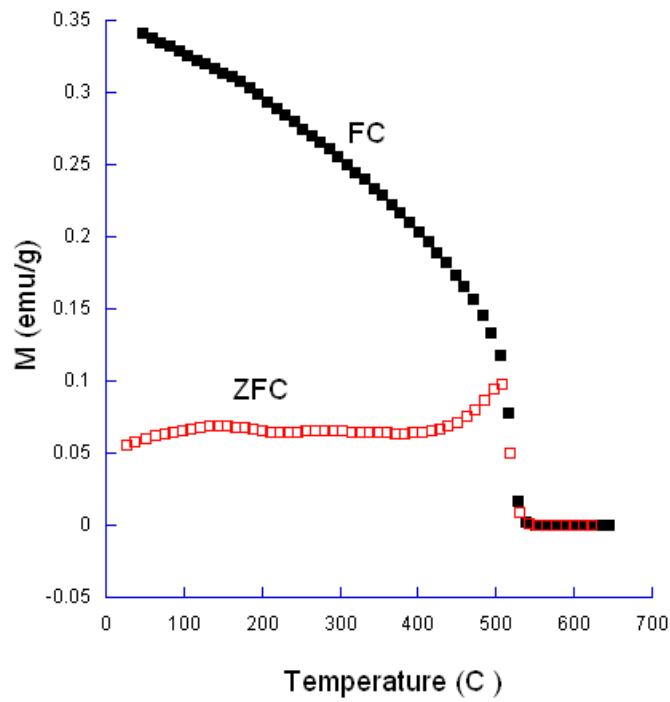


Fig.4.10 M vs. T response for 25%BaTiO<sub>3</sub>-75%CoFe<sub>2</sub>O<sub>4</sub> composite.

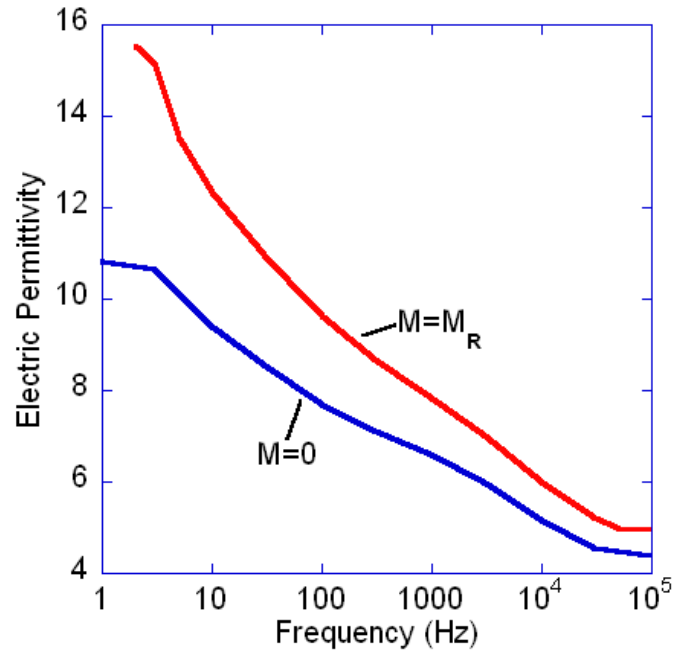


Fig.4.11 DEA for 25%BaTiO<sub>3</sub>-75%CoFe<sub>2</sub>O<sub>4</sub> composite with and without magnetized.

Fig.4.10 shows the M-T behavior of specimen over the range of  $0 < T < 650\text{K}$ . It demonstrates a ferromagnetic phase transition for CoFe<sub>2</sub>O<sub>4</sub> near 505°C. The Curie temperature of the pure CoFe<sub>2</sub>O<sub>4</sub> is almost the same as this composite. It is identified that the composite has the ferromagnetic phase.

#### ***4.5 DEA Measurement***

The dependence of the dielectric constant ( $\epsilon'$ ) with frequency for the composite 25%BaTiO<sub>3</sub>-75%CoFe<sub>2</sub>O<sub>4</sub> is shown in Fig.4.11. The sintered sample was 1 inch in diameter with 1mm thickness. The sample was measured by DEA before and after magnetized. Fig.4.11 show that the electric permittivity increased after the sample was magnetized.

It can be inferred from the result that the magnetization has a huge effect

on the permittivity of the nanocomposite, as the permittivity of magnetized sample is larger than that of the unmagnetized sample. This effect can be explained by the interaction between the ferromagnetic particles and the ferroelectric particles coupling.

#### ***4.6 Discussion***

From the result it can be concluded that most of the research goal has been achieved. Firstly the composite has been made with low expense by sol-gel method. The Curie temperature of ferromagnetic phase in composite was measured as 505°C by VSM which is close to its reported value in literature. Attempts at measuring the Curie temperature of Barium Titanate have been made, but with the limited amount of data, a conclusive result can not be provided yet. The coupling between ferroelectric phase and the ferromagnetic phase was examined through the use of a Dielectric Analyze. An increase of dielectric constant as much as 50% after magnetization was observed.

## Chapter 5: Conclusion

BaTiO<sub>3</sub>-CoFe<sub>2</sub>O<sub>4</sub> biferroic composites have been synthesized by sol-gel method. The synthesis process has been described which consisted of two steps. The first step was to prepare a mixture of the synthesized ferromagnetic and ferroelectric nanoparticles at certain ratio from them into a given shape. The second step was to sinter.

Four samples with different molar ratios were prepared and studied. The precursors of materials have been characterized by DTA and TGA.

X-ray characterization shows that the precursor was of poor crystallinity below 500°C. BaTiO<sub>3</sub> and CoFe<sub>2</sub>O<sub>4</sub> phase were formed at 700°C and 900°C separately. When the sample was sintered at 1100°C, BaTiO<sub>3</sub> and CoFe<sub>2</sub>O<sub>4</sub> phases exist separately as pure and single phase. Four samples were heat-treated at 1100°C for 2 hours. The relative intensities of the patterns of the two phases are indicative of the amount of BaTiO<sub>3</sub>/CoFe<sub>2</sub>O<sub>4</sub> phases.

The average of the particles size for BTO-CFO composite is about 150 nm this was determined by SEM.

We measured the dielectric and magnetic properties of the 25%BaTiO<sub>3</sub>-75%CoFe<sub>2</sub>O<sub>4</sub> composite by DEA, SQUID and VSM. The electric permittivity increased 50% after the sample magnetized. This effect can be explained by the interaction between the ferromagnetic particles and the ferroelectric particles.

The result of VSM shows that the phase transition point of the ferromagnetic phase in 25%BaTiO<sub>3</sub>-75%CoFe<sub>2</sub>O<sub>4</sub> composite is near 505°C.

## Chapter 6: Future Research

### ***6.1 Embedded Particles with Two Phases***

Embedded particles are particles with a ferromagnetic core and ferroelectric exterior layer or vice versa, shown in Fig.6.1. The outer layer directly “grows out” on the core. The advantage of this kind of structure over the sintered sample is that the interaction between these two kinds of materials is stronger than the sintered composite material.

The synthesis process consists of two steps. The first step is to produce nanoparticles of one material by sol-gel method. Then a second layer can be grown by either wet chemical (sol-gel) method or by chemical (CVD) method.

### ***6.2 Films with Embedded Second Phase Particles***

The films with embedded particles are films with embedded particles inside. This kind of structure can be used to make storage media.

The synthesis process consists of three steps. First step is to make nanoparticles by sol-gel method. The second step is to distribute the particles on the surface of substrate. The third step is to deposit film on to the substrate by either dry chemical or wet chemical method.

The other approach to make this kind of structure is to disperse the nanoparticles into the film forming second phase sol solution. Then coat the particle containing sol onto the substrate and form film.



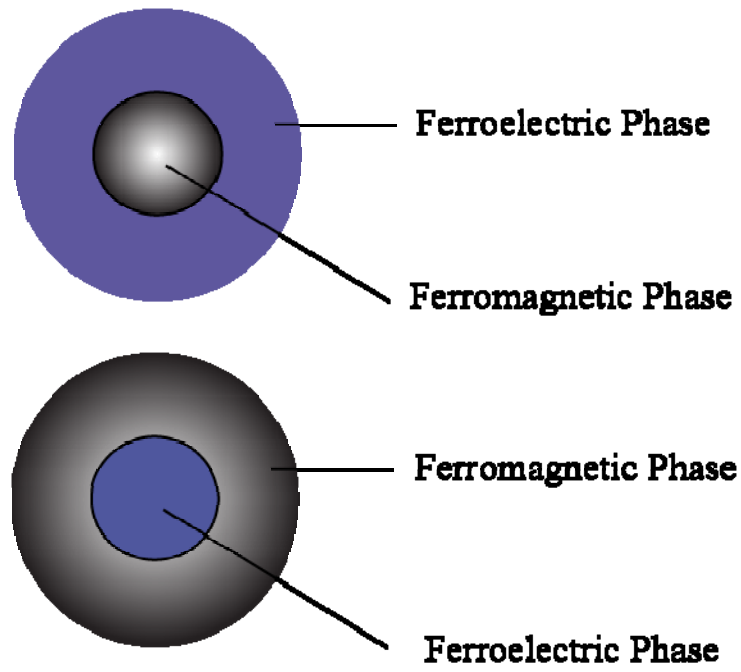


Fig.6.1 Illustration of embedded particles with two phases.

## Appendix:

### XRD analysis data of BaTiO<sub>3</sub>

BaTiO <sub>3</sub>		
Barium Titanium Oxide		
d (Å)	2θ (°)	hkl
7.652	23.22	102
5.492	32.57	110, 104
4.515	39.89	006, 202
3.924	46.21	204
3.524	51.82	116, 212
3.222	57.11	108, 214
2.802	66.69	208, 220
2.643	71.29	217, 311

XRD analysis data of CoFe<sub>2</sub>O<sub>4</sub>

CoFe <sub>2</sub> O <sub>4</sub>		
Cobalt Ferrite		
d (Å)	2θ (°)	hkl
4.847	18.79	111
2.968	30.76	220
2.531	36.1	311
2.424	37.7	222
2.099	43.71	400
1.926	47.64	331
1.713	54.05	422
1.615	57.54	711
1.483	63.13	440
1.419	66.35	531
1.3273	71.48	620
1.2798	74.57	533

## Bibliography:

---

- 1 J.W. Smith and L. E. Cross, "Macroscopic Theory for the Dielectric Properties of Lead Magnesium Niobate", *Ferroelectric* **1** (3), 137-140 (1970).
- 2 K. Ullakko, J.K. Huang, C. Kantner, R.C. O'Handley, and V.V. Kokorin, "Large magnetic-field-induced strains in Ni<sub>2</sub>MnGa single crystals," *Appl. Phys. Lett.* **69**, (1996).
- 3 R. D. James and M. Wuttig, *Phil. Mag. A*, Vol. **77**, No. 5, (1998).
- 4 E. Ascher, H. Rieder, H. Schmid, H. Stossel, *J. Appl. Phys.* **37**: 1404 (1966).
- 5 N. Hur, S. Park, P. A. Sharma, J. Ahn, S. Guha, and S.-W. Cheong, *Nature* (London) **429**, 392 (2004).
- 6 K. Mori and M. Wuttig, *Appl. Phys. Lett.* **81**, 100 (2002).
- 7 J. Ryu, S. Priya, K. Uchino, H. E. Kim, and D. Viehland, *J. Korean Ceramic Society* **39**, 813 (2002). S. Dong, J. Li, and D. Viehland, *Appl. Phys. Lett.* **83**, 2265 (2003).
- 8 Zheng H., Wang J., Lofland S. E., Ma Z., Mohaddes-Ardabili L., Zhao T., Salamanca-Riba L., Shinde S. R., Ogale S. B., Bai F., Viehland D., Jia Y., Schlom D. G., Wuttig M., Roytburd A. and Ramesh R. *Science* **303**, 661 (2004).
- 9 V. E. Wood and A. E. Austin, in *Magnetolectric Interaction Phenomena in Crystals*, A. J. Freeman, H. Schmid, Eds. (Gordon and Breach: Newark, NJ, 1975).

- 
- 10 Y. N. Venentsev, V. V. Gagulin, and I. D. Zhitomirsky, *Ferroelectrics* **73**, 221 (1987).
  - 11 P. Curie, *J. Phys.* 3<sup>e</sup> Ser., 393 (1894).
  - 12 N. Cai, J. Zhai, C. W. Nan, Y. Lin, and Z. Shi, *Phys. Rev. B* **68**, 224103 (2003).
  - 13 J. Ryu, S. Priya, K. Uchino, H. E. Kim, and D. Viehlanf, *J. Korean Ceram. Soc.* **39**, 813 (2002).
  - 14 C. Kittel, *Introduction to Solid State Physics*, New York, (1996).
  - 15 C. C. H. Lo, A. P. Ring, J. E. Snyder and D. C. Jiles *IEEE Trans. Mag.*, **41** (10), 3676 Oct. (2005).
  - 16 Pockels, F. *Abh. Gött* **39**, 1 (1894).
  - 17 *Ferroelectrics and related materials*, Lines and Glass, Oxford (1997).
  - 18 K. Aizu, *J. Phys. Soc. Jpn.* **19**, 918; **20**, 959. *Phys. Rev.* **140**, 590; **146**, 423.
  - 19 D. Berlincourt, *J. Acoust. Soc. Am.* **70**(6), 1586, Dec. (1981).
  - 20 J. Van Suchetelene, *Philips Res. Rep.*, **27**, 28 (1972).
  - 21 K. Uchino, *Ferroelectric Devices* (Marcel Dekker), New York, 255 (2000).
  - 22 Nan, C. Magnetolectric effect in composites of piezoelectric and piezomagnetic phase. *Phys. Rev. B* (Condensed Matter), **50** (9) 6082-8 (1994).
  - 23 D. N. Astrov, *Phys. JETP* **11** 708 (1960).
  - 24 G. T. Rado, *Phys. Rev. Letts.* **6** (11) 609 (1961).
  - 25 G. T. Rado, *Phys. Rev. Letts.* **7** (8) 310 (1961).
  - 26 G. T. Rado, *Phys. Rev. Letts.* **23**(12) 644 (1969).

- 
- 27 D. L. Fox, *Phys. Rev. B* (Condensed Matter), **21**(7) 2926 (1980).
- 28 W. Brixel, *Ferroelectrics* **79** 495 (1988).
- 29 J. P. Rivera, H. Schmid, *J. Phys. Colloq.* **49** 849 (1988).
- 30 H. Tsujino, K. Kohn, *Solid State Communications*, **83**(8) 639 (1992).
- 31 I. Wiegelmann, *Phys. Rev. B* **49**, 10039 (1994).
- 32 J. Van den Boomgaard and R.A.J. Born, *J. Mater. Sci.*, **13**, 1538 (1978).
- 33 J. Ryu, S. Priya, K. Uchino & H. Kim, *J. Elec.* **8**, 107 (2002).
- 34 J.D. MacKenzie. *J Non-Cryst Solids* **48**, 1-10 (1982).
- 35 D.R. Uhlmann, B.J. Zelinski & G.E. Wnek. In: C.J. Brinker, D.E. Clark & D.R. Ulrich (Eds) *Better Ceramics Through Chemistry*. North-Holland, New York, p. 59 (1984).
- 36 <http://www.chemat.com/html/solgel.html>
- 37 S. Q. Ren, L. Q. Weng, S. H. Song, F. Li, *J. Mater. Sci.* **40**, 4375-4378 (2005).
- 38 Van Oosterhout, G.W. *Appl. Sci. Res. Sect. B* **6** 101 (1956).
- 39 H. Young, *PLZT Heterostructures as Transverse Optical Modulators*, Ph.D dissertation, University of Maryland at College Park, 1999.
- 40 Esser, *Gold/Niobium Thin Film Metallizations for GaAs Devices and Circuits*, Ph.D dissertation, University of Maryland at College Park, 2000.